PAPER

Prediction and compensation of magnetic beam deflection in MR-integrated proton therapy: a method optimized regarding accuracy, versatility and speed

IOP Publishing | Institute of Physics and Engineering in Medicine Physics in Medicine & Biology

Phys. Med. Biol. **62** (2017) 1548–1564 doi:10.1088/1361-6560/62/4/1548

Prediction and compensation of magnetic beam deflection in MR-integrated proton therapy: a method optimized regarding accuracy, versatility and speed

Sonja M Schellhammer[1] **and Aswin L Hoffmann**[1,2]

[1] Helmholtz-Zentrum Dresden-Rossendorf, Institute of Radiooncology, Händelallee 26, 01309 Dresden, Germany
[2] Department of Radiotherapy and Radiooncology, University Hospital Carl Gustav Carus at the Technische Universität Dresden, Dresden, Germany

E-mail: s.schellhammer@hzdr.de

Received 1 April 2016, revised 4 September 2016
Accepted for publication 4 November 2016
Published 25 January 2017

Abstract

The integration of magnetic resonance imaging (MRI) and proton therapy for on-line image-guidance is expected to reduce dose delivery uncertainties during treatment. Yet, the proton beam experiences a Lorentz force induced deflection inside the magnetic field of the MRI scanner, and several methods have been proposed to quantify this effect. We analyze their structural differences and compare results of both analytical and Monte Carlo models. We find that existing analytical models are limited in accuracy and applicability due to critical approximations, especially including the assumption of a uniform magnetic field. As Monte Carlo simulations are too time-consuming for routine treatment planning and on-line plan adaption, we introduce a new method to quantify and correct for the beam deflection, which is optimized regarding accuracy, versatility and speed. We use it to predict the trajectory of a mono-energetic proton beam of energy E_0 traversing a water phantom behind an air gap within an omnipresent uniform transverse magnetic flux density B_0. The magnetic field induced dislocation of the Bragg peak is calculated as function of E_0 and B_0 and compared to results obtained with existing analytical and Monte Carlo methods. The deviation from the Bragg peak position predicted by Monte Carlo simulations is smaller for the new model than for the analytical models by up to 2 cm. The model is faster than Monte Carlo methods, less assumptive than the analytical models and applicable to realistic magnetic fields. To compensate for the predicted Bragg peak dislocation, a numerical optimization strategy is introduced and evaluated. It includes an adjustment of both the proton beam entrance angle

and energy of up to 25° and 5 MeV, depending on E_0 and B_0. This strategy is shown to effectively reposition the Bragg peak to its intended location in the presence of a magnetic field.

Keywords: proton therapy, image-guided radiotherapy, IGPT, magnetic resonance imaging, MR guidance, beam trajectory prediction, RAMDIM

(Some figures may appear in colour only in the online journal)

1. Introduction

Proton therapy is a type of external beam radiation treatment that uses high-energy protons to treat cancer. As compared to photon-based radiotherapy, its main advantage lies in the pronounced dose maximum, the Bragg peak, which is energy-dependent in depth and bordered by steep dose gradients, especially at the distal edge (Jäkel 2009). However, the gradients also make the dose distribution very sensitive to inter- and intrafractional uncertainties resulting from setup errors and anatomical variations (i.e. organ motion and deformation), which gives rise to considerable range uncertainties (Lomax 2008).

The aim of real-time image-guided radiotherapy is to reduce these uncertainties by imaging essential parts of the patient anatomy in treatment position during irradiation. Thus, tissue motions and deformations can be tracked and dynamic beam delivery with enhanced dose conformality and reduced safety margins is rendered possible. Magnetic resonance imaging (MRI) has been suggested to be a promising candidate for this task, offering a fast real-time imaging modality with excellent soft tissue contrast without using ionising radiation for image formation (Raaymakers *et al* 2008). The concept feasibility to integrate MRI with photon-based radiotherapy into a hybrid system has been shown by several research groups in the Netherlands (Lagendijk *et al* 2014a), Canada (Fallone 2014) and Australia (Keall *et al* 2014). Because of the increased geometrical sensitivity of proton therapy, this technique is expected to profit even more from an integration with MRI.

So far, MR-integrated proton therapy (MRiPT) has only been described as a hypothetical modality in simulation studies (Raaymakers *et al* 2008, Wolf and Bortfeld 2012, Moteabbed *et al* 2014, Hartman *et al* 2015, Li 2015, Moser 2015, Oborn *et al* 2015). Likewise challenging as in MR-integrated photon therapy, there are specific technological and physical problems that need to be solved when facing MRiPT. For example, there will be mutual interactions between the magnetic field of the MRI scanner and that of the beam transport magnets and the beam steering and monitoring system (Schippers and Lomax 2011). Probably more problematic is the fact that, being charged particles, the therapeutic protons will be deflected by the magnetic field of the MRI scanner (Oborn *et al* 2016). Different studies have focussed on quantifying the beam deflection effect for dosimetric and treatment planning purposes using particle tracking with Monte Carlo simulations (Raaymakers *et al* 2008, Moteabbed *et al* 2014, Li 2015, Moser 2015, Oborn *et al* 2015) or analytical models (Wolf and Bortfeld 2012, Hartman *et al* 2015).

As pointed out by Oborn *et al* (2015), the general consensus from these works is that the proton beam deflection within a patient or water phantom is predictable and so essentially correctable during treatment planning stages. However, different approaches have been introduced to assess this effect, and neither their structural differences nor their degree of accordance have been analyzed. Differences can be expected, since all approaches are subject to their respective shortcomings. For instance, previously published analytical models imply critical assumptions, and are only applicable to the simplified case of a uniform (i.e. unrealistic)

magnetic field. Monte Carlo simulations are potentially more accurate, but very time-consuming, which inhibits their use for routine treatment plan optimization and real-time treatment plan adaption. Thus, a method is required to quantify and correct for the deflection, which is optimized towards accuracy, versatility and calculation time.

The aim of the current work therefore is three-fold. Firstly, we analyze and compare results published so far in terms of dosimetric accuracy and discuss the limitations of the different methods. Secondly, we present a new model to estimate the trajectory of a mono-energetic proton beam traversing a water/air phantom inside a uniform transverse magnetic field and evaluate its performance against results of the previous models. We call this model Raytracing Algorithm for Magnetic Deflection of Ions in Media, short RAMDIM. Thirdly, we use RAMDIM to introduce a fast and accurate beam correction strategy for repositioning the Bragg peak to its intended location in the presence of the magnetic field. To help understand the limitations of previously published analytical models, a condensed review and analysis thereof is given in section 2. On this basis, RAMDIM is presented in section 3. The setup for the subsequent evaluation and comparison of this model in relation to existing approaches is detailed in section 4. Obtained results are given in section 5. In section 6, the main findings and most important implications are discussed. A short conclusion and outlook to further investigations are provided in section 7.

2. Analysis of existing analytical models

For a better understanding of the following chapters, previously published analytical models are shortly reviewed in this section. Being first order approaches, the methods model a mono-energetic proton beam traversing a simple water/air phantom inside a uniform transverse magnetic field.

2.1. General considerations

Consider a uniform magnetic field in vacuum of flux density $\vec{B} = B_0 \cdot \vec{e}_z$ which is aligned parallel to the z axis and translation invariant. Let a mono-energetic proton pencil beam of kinetic energy E_0 with an initial velocity $\vec{v}_0 = v_0 \cdot \vec{e}_x$ perpendicular to $\vec{B}$ traverse the field (see figure 1(a)). The entrance velocity $v_0 = c \cdot \sqrt{\frac{E_0(E_0+2m_0c^2)}{(E_0+m_0c^2)^2}}$ is connected to E_0 through the proton rest mass m_0 and the speed of light c. Carrying the elementary electric charge q, the proton's equation of motion is governed by the Lorentz force

$$\vec{F} = \frac{\mathrm{d}\vec{p}}{\mathrm{d}t} = \gamma m_0 \frac{\mathrm{d}\vec{v}}{\mathrm{d}t} + m_0 \vec{v} \frac{\mathrm{d}\gamma}{\mathrm{d}t} = q(\vec{v} \times \vec{B}) \tag{1}$$

with the relativistic momentum $\vec{p} = \gamma m_0 \vec{v}$ and the Lorentz factor $\gamma = \frac{1}{\sqrt{1-(\frac{v_0}{c})^2}}$. As v_0 is constant, which yields $\frac{\mathrm{d}\gamma}{\mathrm{d}t} = 0$, this differential equation has a simple analytical solution

$$v_x = v_0 \cos\left(\frac{qB_0}{\gamma m_0} t\right),\ v_y = v_0 \sin\left(\frac{qB_0}{\gamma m_0} t\right),\ v_z = 0 \tag{2}$$

for the velocity components v_x, v_y and v_z in x-, y- and z-direction, respectively. The protons thus move in a circular course with an angular frequency $\omega_0 = \frac{qB_0}{\gamma m_0}$. The radius of this course, the gyroradius, is given by

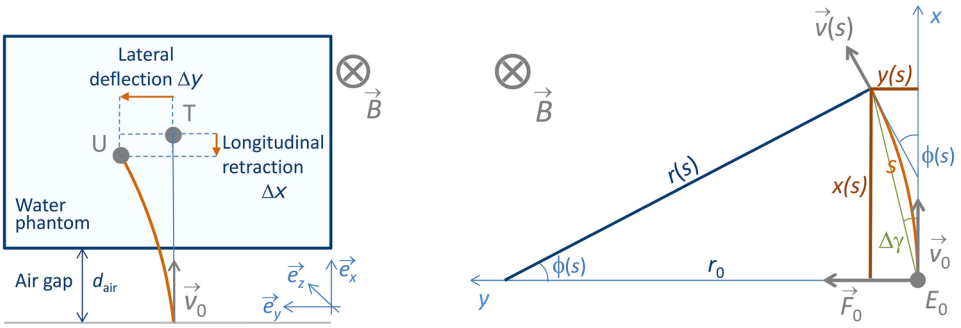

Figure 1. Setup geometry with omnipresent uniform transverse magnetic field $\vec{B}$. Starting from the beam nozzle, the proton beam (orange) traverses an air gap of length d_{air} before entering a water phantom. It is deflected by the magnetic field resulting in a deflection and retraction from its intended Bragg peak position T to the position U (a). The geometrical representation of the beam trajectory (b) is discussed in the text.

$$r = \frac{v_0}{\omega_0} = \frac{\gamma m_0 v_0}{qB_0}. \tag{3}$$

Now consider a setup geometry with a water phantom placed inside a virtual gantry-based MRiPT system. The distance between the proton beam nozzle and the water phantom's surface is denoted by d_{air}. As opposed to the vacuum situation, protons deposit energy when traversing media until stopping at a finite range R_0. The range in water can be approximated by a power-law range-energy relationship (Bortfeld 1997)

$$R_0 = \alpha E_0^p \tag{4}$$

with $p \approx 1.75$ and $\alpha \approx 2.43 \times 10^{-3}\,\text{MeV}^{-\text{p}}\,\text{cm}$ (Wolf and Bortfeld 2012). The protons slow down quasi continuously (ICRU 1993) and hence the gyroradius decreases with increasing depth according to equation (3), which leads to a curled-up beam trajectory. Consequently, the Bragg peak experiences both a lateral deflection Δy from the beam's entrance direction $\vec{e}_x$ and a longitudinal retraction Δx from its expected depth (see figure 1(a)).

2.2. Analytical integration model (AI model)

The authors of the first analytical model (Wolf and Bortfeld 2012) have assessed the Bragg peak deflection and retraction by an analytical integration of geometric deflection steps. In accordance with figure 1(b) and equation (3), they have described the deflection angle ϕ between the particle motion and the x axis by

$$\frac{\mathrm{d}\phi}{\mathrm{d}s} = \frac{1}{r(s)} = \frac{qB_0}{\gamma(s) m_0 v(s)} \tag{5}$$

with the gyroradius $r(s)$, the relativistic velocity $v(s)$ and the Lorentz factor $\gamma(s) = \frac{1}{\sqrt{1-(\frac{v(s)}{c})^2}}$ as functions of the travelled distance s along its curved path. A small angle approximation $\frac{\mathrm{d}y}{\mathrm{d}s} = \sin\phi(s) \approx \phi(s)$ has been applied, yielding the lateral deflection as function of s

$$y(s) = \int_0^s \phi(s')\mathrm{d}s'. \tag{6}$$

The deflection at the end of the trajectory in a water phantom without air gap (i.e. $d_{\mathrm{air}} = 0$) has thus been obtained by analytical integration as

$$\begin{aligned}\Delta y &= y(s = R_0)\\ &= \frac{7}{30}\frac{qB_0\alpha^2}{\sqrt{2m_0}}(2m_0c^2)^3\left[\sqrt{1+\frac{E_0}{2m_0c^2}}\left(3\left(\frac{E_0}{2m_0c^2}\right)^2 - 4\left(\frac{E_0}{2m_0c^2}\right)+8\right)-8\right].\end{aligned} \tag{7}$$

In an analogous manner, the longitudinal position $x(s)$ has been obtained by assuming $\frac{\mathrm{d}x}{\mathrm{d}s} = \cos\phi(s) \approx 1 - \frac{\phi(s)^2}{2}$ which yields

$$x(s) = s - \frac{1}{2}\int_0^s \phi^2(s')\mathrm{d}s'. \tag{8}$$

This term has been treated non-relativistically (i.e. $\gamma = 1$ and $v(s) = \sqrt{\frac{2E(s)}{m_0}}$) and thus the overall retraction length was quantified by

$$\Delta x = R_0 - x(R_0) = \frac{q^2B_0^2\alpha^3E_0^{3p-1}}{2m_0}\,\frac{2p^2}{(4p-1)(3p-1)}. \tag{9}$$

The model was stated to be applicable to slab phantom geometries of arbitrary material thickness and composition by addition of the deflections obtained in each layer. For air gaps, energy loss has been assumed to be negligible, yielding

$$d_{\mathrm{air}} = x_{\mathrm{air}}(s) = s - \frac{q^2B_0^2s^3}{12m_0E_0} \text{ and } y_{\mathrm{air}}(s) = \frac{qB_0s^2}{2\sqrt{2m_0E_0}}. \tag{10}$$

An advantage of the AI model is that the whole curved beam trajectory can be calculated from $x(s)$ and $y(s)$, which is important for treatment planning and dosimetric verification. However, the model cannot be easily adapted to realistic, inhomogeneous magnetic fields mainly because of the pathlength parametrization, but also due to the need for an analytical description of the magnetic flux density distribution.

2.3. Trigonometric model (TG model)

In the work of Wolf and Bortfeld (2012), no concrete compensation strategy for the beam deflection has been proposed. This problem has been adressed by a more recent paper (Hartman *et al* 2015). Here, a simplified analytical model has been introduced in order to propose a beam deflection correction strategy. Several assumptions have been made to enable a direct trigonometric quantification of the proton beam deflection without the use of more complex methods such as integration. Firstly, the change of the gyroradius due to energy loss in matter has been neglected, i.e. $r(s) = r_0$. Secondly, longitudinal beam retraction was not taken into account, i.e. $\Delta x = 0$ and $x(s = R_0) = R_0$. Following these approximations and figure 1(b), the lateral deflection in the water phantom (with $d_{\mathrm{air}} = 0$) has been expressed as

$$\Delta y = r_0\left(1 - \cos\left[\arcsin\left(\frac{R_0}{r_0}\right)\right]\right), \tag{11}$$

which can be simplified to

$$\Delta y = r_0 - \sqrt{r_0^2 - R_0^2}. \tag{12}$$

As a third approximation, the proton motion was assumed to be non-relativistic ($\gamma = 1$ and $v(s) = \sqrt{\frac{2E(s)}{m}}$), which yields a (constant) gyroradius of

$$r_0 = \frac{\sqrt{2mE_0}}{qB_0} \approx 14.4\frac{\sqrt{E_0}}{B_0}\,\mathrm{T\ cm\ (MeV)}^{-\frac{1}{2}}. \tag{13}$$

The airgap of thickness d_{air} in front of the water phantom has been accounted for by replacing R_0 with $(R_0 + d_{\mathrm{air}})$, assuming that energy loss in air is negligible.

A correction strategy for the deflection has been proposed by applying an angle correction to the entrance direction $\vec{v}_0$ of the beam. According to figure 1(b), it was obtained by

$$\Delta\gamma = \arctan\left(\frac{y(R_0)}{x(R_0)}\right) = \arctan\left(\frac{\Delta y}{R_0}\right). \tag{14}$$

The authors stated that this angle correction could be implemented either by pencil beam scanning magnets or by an isocentric gantry rotation around the phantom.

2.4. Summary

Although both the AI and the TG model offer a reasonable first approach to the problem of magnetic proton beam deflection in a transverse uniform magnetic field, they have their respective shortcomings. The AI model relies on a small angle approximation which is problematic for large deflection angles, treats retraction non-relativistically and does not offer a compensation strategy for the Bragg peak deflection. The TG model neglects relativistic effects, beam retraction and the decreasing gyroradius as a function of penetration depth. Neither the AI nor the TG model seems applicable to a realistic, i.e. non-uniform, magnetic field and patient anatomy. Aiming to provide a solution which is more accurate and versatile than these two models, but faster than Monte Carlo approaches, we therefore present and verify an alternative model in the following sections.

3. New model formulation

The model we propose is an iterative analytical method to reconstruct the trajectory of a mono-energetic proton beam based on first physics principles and geometrical considerations. It contains less critical approximations than currently available analytical models and offers a correction strategy for the predicted beam deflection and retraction. It is called Raytracing Algorithm for Magnetic Deflection of Ions in Media (RAMDIM).

3.1. Incremental reconstruction of the proton beam trajectory

Consider the geometry presented in section 2 and figure 2 and let the proton beam's entry position to the magnetic field be $\vec{x}_0 = (x_0, y_0, z_0)$. The initial gyroradius caused by the magnetic field is (see equation (3))

$$r_0 = \frac{\gamma m_0 v_0}{qB_0} = \frac{\sqrt{2m_0E_0(1 + \frac{E_0}{2m_0c^2})}}{qB_0}. \tag{15}$$

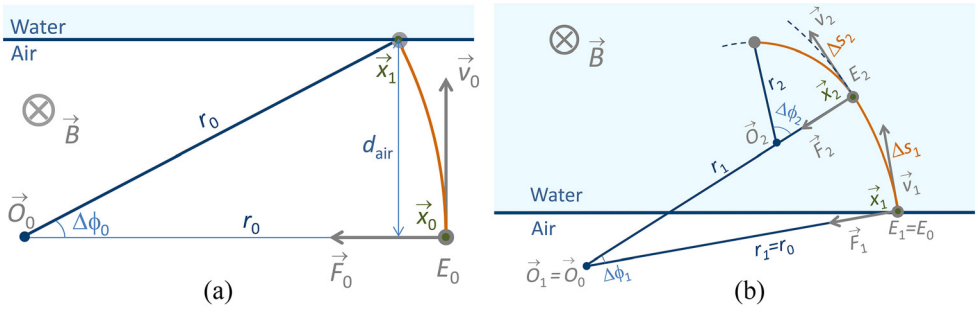

Figure 2. Geometrical representation of the proposed model (RAMDIM). The proton beam deflection in air is calculated trigonometrically assuming no energy loss (a), whereas a changing gyroradius due to energy loss is taken into account in water (b). Symbols are explained in the text.

The first relevant point of the trajectory is the entrance position of the proton beam at the surface of the water phantom $\vec{x}_1$. Energy loss inside the airgap is considered to be negligible, therefore $\vec{x}_1$ is obtained by

$$\vec{x}_1 = \boldsymbol{R}(\Delta\phi_0) \cdot \vec{x}_0, \tag{16}$$

with the rotation matrix $\boldsymbol{R}(\Delta\phi_0)$ rotating the point $\vec{x}_0$ counterclockwise through an angle $\Delta\phi_0$ about the center of rotation $\vec{O}_0 = (x_0, y_0 + r_0, z_0)$ (see figure 2(a)). $\Delta\phi_0$ satisfies

$$\Delta\phi_0 = \arcsin\left(\frac{d_{\text{air}}}{r_0}\right). \tag{17}$$

Inside the water phantom, energy loss is modeled by the continuous slowing down approximation (ICRU 1993) and discretized into small steps of constant energy and hence constant gyroradius (see figure 2(b)). The energy step size ε is chosen for every simulation such that the studied parameters, i.e. Δy, Δx and the correction parameters, are independent of ε within the decimal precision they are given in. Following equation (4), for each energy step i ($i = 1, ..., n$ with $n = \lfloor \frac{E_0}{\varepsilon} \rfloor$) the travelled path length in water, s_i, can be calculated from (see equation (4))

$$s_i = R_0 - \alpha E_i^p, \tag{18}$$

which results in an incremental deflection angle of

$$\Delta\phi_i = \frac{s_{i+1} - s_i}{r_i} = \frac{\Delta s_i}{r_i} \tag{19}$$

with the energy-dependent gyroradius $r_i = \frac{\sqrt{2m_0E_i(1 + \frac{E_i}{2m_0c^2})}}{qB_0}$ (in analogy to equation (15)). The next particle position $\vec{x}_{i+1}$ is obtained by applying the rotational matrix of angle $\Delta\phi_i$ to $\vec{x}_i$, i.e. $\vec{x}_{i+1} = \boldsymbol{R}(\Delta\phi_i) \cdot \vec{x}_i$. Here, the center of rotation $\vec{O}_i$ is determined by (see figure 2(a))

$$\vec{O}_i = \frac{r_i}{|\vec{O}_{i-1} - \vec{x}_i|}(\vec{O}_{i-1} - \vec{x}_i). \tag{20}$$

Thus, the proton trajectory is fully reconstructed until reaching the Bragg peak at step $i = n$. The overall deflection Δy and retraction Δx are then obtained as the projections of the difference between the Bragg peak positions $\vec{x}_n$ with and without magnetic field. It was

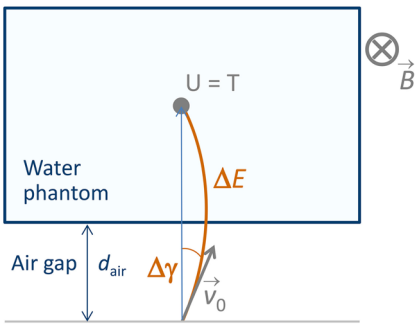

Figure 3. The proposed correction algorithm includes a correction of the proton energy ΔE_0 and entrance angle $\Delta\gamma$ such that the actual Bragg peak location U coincides with the intended position T.

verified that the total traveled pathlength is equal to the proton range within 0.1 mm accuracy, i.e. $s_n - R_0 < 0.1$ mm.

Since in reality both the MR magnetic field and the patient anatomy are non-homogeneous, it is important to mention that, as opposed to existing analytical models, this method is applicable to position-dependent magnetic flux densities and material characteristics. As the particle position $\vec{x}_i$ is calculated in each iteration step, this can be realized for example by reading the magnetic flux density or the material-dependent proton range from a lookup table in each step. The proton range in different materials can be calculated by fitting the range-energy relationship (equation (4)) to tabulated stopping power data (ICRU 1993). For example, a fit for cortical bone yields $p \approx 1.759$ and $\alpha \approx 2.56 \times 10^{-3}\,\mathrm{MeV}^{-\mathrm{p}}\,\mathrm{cm}$ (Lühr *et al* 2012).

The algorithm has been realised in MATLAB (Release 2015b, The MathWorks, Inc., Natick, Massachusetts, United States).

3.2. Correction strategy

As an advancement to the TG model, we propose a correction strategy that simultaneously adjusts the proton beam entrance angle and energy (see figure 3). The angle correction $\Delta\gamma$ compensates for the lateral deflection of the Bragg peak and can only be applied by pencil beam scanning magnets. The energy correction ΔE_0 accounts for the retraction caused by the path curvature and has not been considered before. Both correction parameters are optimized such that the distance to agreement (DTA) between the corrected Bragg peak position $\vec{x}_{n,\mathrm{corr}} = \vec{x}_n(\vec{B}, \gamma_0 + \Delta\gamma, E_0 + \Delta E_0)$ and the intended position $\vec{x}_{n,0} = \vec{x}_n(0\,\mathrm{T}, \gamma_0, E_0)$

$$\mathrm{DTA} = \left|\vec{x}_{n,\mathrm{corr}} - \vec{x}_{n,0}\right| \tag{21}$$

is minimized. This bi-parameter optimization is performed numerically using the MATLAB Optimization Toolbox function `fminsearch`, which implements the simplex search method (Lagarias *et al* 1998).

As an alternative to the angle correction, a patient shift has been suggested by Moteabbed *et al* (2014). However, the deflection of a single Bragg peak strongly depends on the beam energy, entrance angle and the irradiated geometry, and therefore cannot completely be compensated for by a constant shift. For the same reason, we agree with Oborn *et al* (2015) that MRiPT can presumably only be realized using a pencil beam scanning technique.

4. Setup and parameter choice

The new method (RAMDIM, as described in section 3) has been used to predict the trajectories of mono-energetic proton pencil beams of energies E_0 between 60 MeV and 250 MeV in a uniform transversal magnetic field of magnetic flux density B_0. Selected examples for B_0 were 0.5 T as a commonly used flux density in open MRI systems, 1.5 T as typical value for diagnostic images, and 3 T because of its allowance for very fast sequences, which are important for on-line image-guidance (Lagendijk *et al* 2014b). The trajectories were studied in two different geometries: one with a water phantom alone, and one with an air gap between the phantom and the beam nozzle of thickness d_{air}. The parameter $d_{\text{air}} = 25$ cm was chosen by way of example as a typical distance between the beam nozzle and the patient.

The lateral deflection Δy and longitudinal retraction Δx were calculated as functions of E_0 and B_0 with both the new model (RAMDIM) and the two analytical models (AI and TG, as discussed in section 2). Currently being the most accurate method for proton trajectory prediction, published values obtained by Monte Carlo particle tracking (Raaymakers *et al* 2008, Moteabbed *et al* 2014, Li 2015, Moser 2015) were compared to the results gained with the three models. Furthermore, RAMDIM's capability to handle anatomical heterogeneities is demonstrated exemplarily by calculating the proton beam trajectory in a phantom consisting of both bone and water. Correction parameters $\Delta\gamma$ and ΔE_0 in water were calculated and compared to the TG method, and beam trajectories obtained with both correction methods were reconstructed in order to evaluate whether a distance remains to the intended Bragg peak position.

The required decimal precision of results was chosen to be 0.1 mm for Δx and Δy, 0.1° for $\Delta\gamma$, and 0.1 MeV for ΔE_0. Accordingly, the energy step size ε was reduced until these parameters were constant on the first decimal place, yielding a required step size of $\varepsilon = 0.1$ MeV. This corresponds to a steplength in water Δs (see equations (18) and (19)) of up to 0.3 mm for high proton energies ($E_i = 250$ MeV) and down to 4×10^{-4} mm for low energies ($E_i = 0.1$ MeV).

Calculations were carried out on a PC workstation with 8 GB RAM and a 64 bit Intel Core i3-3220 dual core processor running at 3.3 GHz. The calculation for one experiment (defined by E_0, B_0 and d_{air}) took less than 0.07 s for Δx and Δy, and less than 28 s for $\Delta\gamma$ and ΔE_0 for all studied energies and magnetic flux densities.

5. Results

5.1. Bragg peak deflection and retraction

We first compare results obtained with our model (RAMDIM) to those of the two analytical models discussed in section 2. A discussion of differences and an interpretation of results follow in section 6.

Figure 4(a) depicts the Euclidean distance of Bragg peak positions obtained by the AI and TG model to those obtained with RAMDIM in water. As can be appreciated from this figure, the distance increases with increasing energy and magnetic flux density from 0 cm for 60 MeV and 0.5 T up to 2.1 cm for the TG model and 0.4 cm for the AI model at 250 MeV and 3 T.

For a comparison of the models inside the air gap, the difference in water phantom entrance positions behind an air gap of thickness $d_{\text{air}} = 25$ cm are depicted in figure 4(b). The distance to the TG model's results increases with increasing proton energy up to 2.8 mm for 250 MeV and 3 T. As opposed to that, for the AI model it increases with decreasing energy up to 4.8 mm at 60 MeV and 3 T.

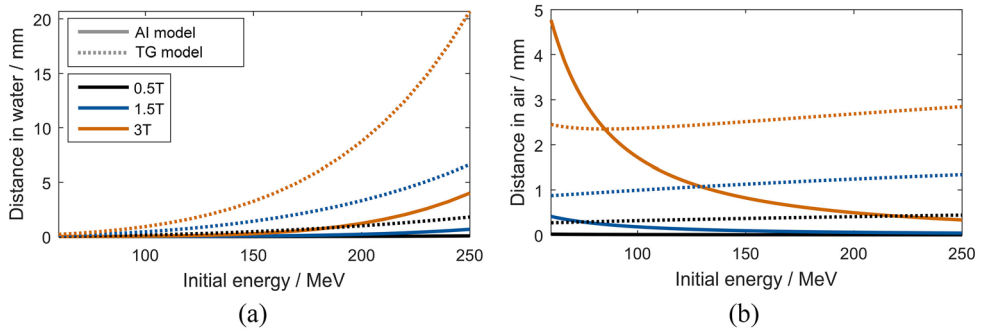

Figure 4. Euclidean distance between positions calculated with previously published analytical models and with the new model. (a): Distance in water between Bragg peak positions inside the phantom alone, (b): distance in air of beam entrance position to the water phantom behind an airgap of $d_{\mathrm{air}} = 25$ cm.

In the next step, we compare AI, TG and RAMDIM to published results obtained by Monte Carlo particle tracking in a water phantom ($d_{\mathrm{air}} = 0$). An overview of calculated deflection and retraction values Δy and Δx in water is given for different uniform magnetic flux densities and beam energies in table 1. Differences of the three analytical models to the reference results are displayed in figure 5.

For all the models, the differences increase with increasing proton energy and magnetic flux density. This can be expected, as Δx and Δy increase with increasing path length and Lorentz force, so that differences due to approximations become more pronounced. However, deviations of the three models behave differently from each other.

For the AI model, the lateral deflection Δy agrees within 2.5 mm with Monte Carlo reference results up to proton energies of 200 MeV for all B_0 considered, but only within 8 mm for 250 MeV at 3 T. The calculated longitudinal retraction Δx agrees within 1.5 mm with the reference for all studied setups, except for 250 MeV and 3 T (3 mm). Here, the lateral deflection tends to be overestimated, whereas retraction by trend seems to be underestimated.

For the TG model, the deflection Δy agrees with Monte Carlo results within 2 mm for all setups except for 200 MeV and 1.5 T, and 250 MeV and 3 T, where the deviations amount to 3.2 mm and 4.2 mm, respectively. The TG model tends to underestimate Δy. The full neglection of the longitudinal retraction of the Bragg peak leads to differences in Δx of up to 2.1 cm for 250 MeV and 3 T.

Results obtained with RAMDIM show an agreement with the reference results in Δy within 2 mm for all studies setups, except for 250 MeV at 1.5 T (2.6 mm) and 3 T (4.6 mm). The retraction Δx agrees within 1.5 mm for all studied energies and magnetic flux densities. The model shows a trend of overestimating lateral deflection and underestimating longitudinal retraction.

A statistical comparison of the accuracy of the three models in relation to the Monte Carlo results is displayed in figure 6. Regarding the lateral deflection Δy, the three models show only small differences in both median and average deviation, which amount to 0.5 mm and 1 mm, respectively. However, the upper percentiles (i.e. 75% and 91%) deviate stronger from zero for the TG model than for the other two models, and the AI model shows a strong outlier of 8 mm at 250 MeV and 3 T. For the longitudinal retraction Δx, the median and average deviation of RAMDIM and the AI model are comparably low (below 1 mm), but only RAMDIM shows a smaller 91%-percentile and no outlier. As retraction is neglected in the TG model, all studied statistical measures are highly increased as compared to the two other models. The sample

Table 1. Predicted lateral deflection Δy and longitudinal retraction Δx of a mono-energetic proton beam with initial energy E_0 at the Bragg peak. The beam traverses a water phantom ($d_{air} = 0$) in a uniform transverse magnetic field of flux density B_0. Results are given for the new method (RAMDIM) and the AI and TG models (equations (7), (9) and (11)) in relation to published Monte Carlo results (ref.).

		Δy /mm				Δx /mm			Reference (ref.)
B_0/T	E_0/MeV	RAMDIM	AI	TG	ref.	RAMDIM	AI	ref.	
0.35	60	0.2	0.2	0.2	0.2	0.0	0.0	0.0	Moser (2015)
	150	2.7	2.7	2.4	2.5	0.0	0.0	0.1	Moser (2015)
	250	12.4	12.4	11.2	11.8	0.3	0.3	1.2	Moser (2015)
0.5	90	0.9	0.9	0.8	1.0				Raaymakers *et al* (2008)
	90				1.2				Moteabbed *et al* (2014)
	200	9.2	9.2	8.2	10.0				Moteabbed *et al* (2014)
1.0	60	0.5	0.5	0.4	0.5	0.0	0.0	0.0	Moser (2015)
	150	7.8	7.8	6.9	7.3	0.3	0.3	1.5	Moser (2015)
	250	35.4	35.5	32.3	32.8	2.3	2.6	3.5	Moser (2015)
1.5	90	2.6	2.6	2.2	3.0				Moteabbed *et al* (2014)
	200	27.4	27.5	24.8	28				Moteabbed *et al* (2014)
3.0	60	1.5	1.5	1.3	1.4	0.1	0.1	0.1	Moser (2015)
	90	5.1	5.1	4.5	5.0				Raaymakers *et al* (2008)
	120	12.0	12.1	10.7	11.0	1.0	1.0	2.0	Li (2015)
	150	23.2	23.5	21.1	22.8	2.5	2.6	3.5	Moser (2015)
	180	39.7	40.3	36.9	38	5.3	5.7	6.0	Li (2015)
	250	103.4	106.6	103.1	98.9	20.7	23.1	20.5	Moser (2015)

size for this inter-model comparison has been limited to 11 and 16 data points for retraction and deflection, respectively.

RAMDIM's capability to predict the proton beam trajectory in heterogeneous media is demonstrated in figure 7. A 250 MeV proton beam traversing a water phantom with a 10 cm bone insert has been modeled in a field of $B_0 = 3$ T. As expected, the proton range is reduced according to equation (4). Additionally, for the same depth, the curvature of the beam behind the bone insert is stronger than in a homogeneous water phantom due to the increased energy loss in bone. In the same manner, arbitrary geometries can be studied using this model.

5.2. Beam correction parameters

To compensate for the deflection of the Bragg peak, calculated correction parameters $\Delta\gamma$ and ΔE_0 are presented for different proton energies E_0 and magnetic flux densities B_0 in table 2. The beam energy correction calculated with RAMDIM ranges from $\Delta E_0 = 0.1$ MeV (0.2%) for 60 MeV and 0.5 T up to $\Delta E_0 = 4.7$ MeV (2%) for 250 MeV and 3 T. The angle correction ranges from $\Delta\gamma = 3.6°$ for 60 MeV and 0.5 T up to $\Delta\gamma = 24.4°$ for 250 MeV and 3 T. The difference to the correction angle from the TG model is smaller than 0.5° for magnetic flux densities up to 1.5 T, but exceeds to 3.8° (16%) at 250 MeV and 3 T.

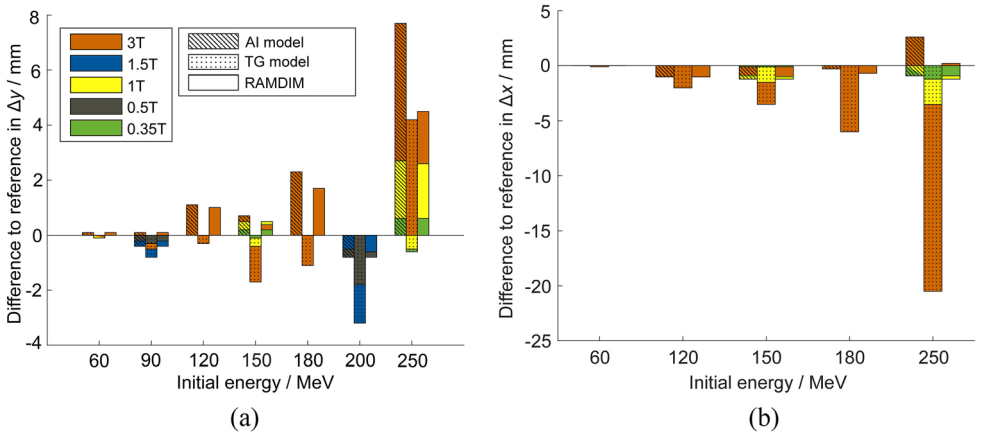

Figure 5. Difference in Bragg peak deflection Δy and retraction Δx between results of the analytical models and Monte Carlo results for the studied set of proton energies and magnetic flux densities (see table 1). Positive values indicate an overestimation of the three models in relation to the particle tracking results, and negative values indicate an underestimation. Colored bars individually span from zero (i.e. no stacking).

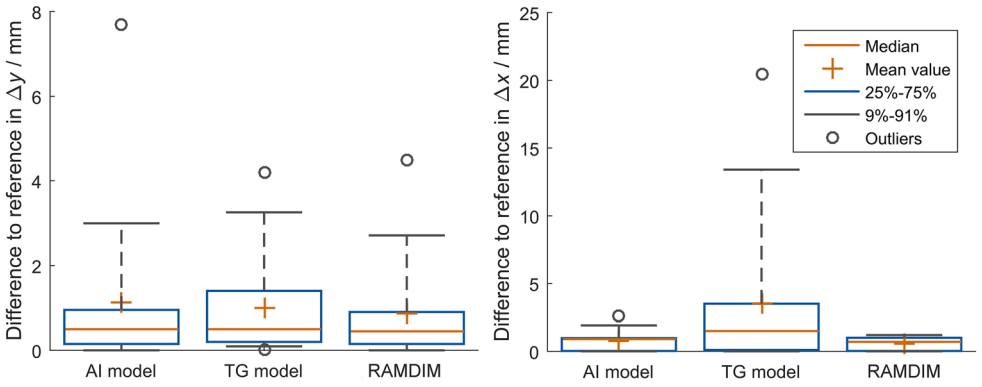

Figure 6. Boxplots of absolute differences in Bragg peak deflection Δy and retraction Δx between the different models and Monte Carlo reference results (see table 1).

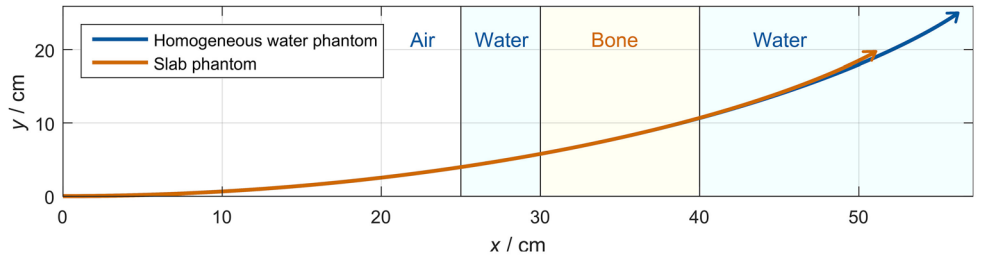

Figure 7. 250 MeV proton beam trajectory in a magnetic field of 3 T through different phantoms behind an airgap of $d_{\text{air}} = 25$ cm calculated with RAMDIM. Blue: homogeneous water phantom, orange: slab phantom with bone insert of 10 cm thickness. The Bragg peak position is indicated by the arrowhead of the trajectory.

Table 2. Beam energy and angle correction parameters for different initial energies and magnetic flux densities for a distance between the phantom surface and the entrance position of the beam to the magnetic field of $d_{\text{air}} = 25$ cm.

		RAMDIM		TG model
B_0 /T	E_0 /MeV	ΔE_0 /MeV	$\Delta\gamma$ /°	$\Delta\gamma$ /°
0.5	60	0.1	3.6	3.3
	100	0.1	3.2	3.3
	150	0.1	3.3	3.3
	200	0.1	3.6	3.6
	250	0.1	4.0	4.0
1.5	60	0.5	10.7	11.1
	100	0.5	9.6	10.0
	150	0.6	9.8	10.1
	200	0.8	10.7	11.0
	250	1.1	12.0	12.3
3	60	2.0	21.5	24.6
	100	2.1	19.3	21.5
	150	2.5	19.7	21.9
	200	3.3	21.6	24.3
	250	4.7	24.4	28.2

As an example, proton trajectories modelled with RAMDIM for both correction parameter sets are depicted for $E_0 = 200$ MeV and $B_0 = 3$ T in figure 8. As the correction method of the TG model does not include an energy correction, the Bragg peak retraction is not compensated for. Additionally, the lateral deflection Δy is overcompensated by a too large correction angle. Therefore, the DTA between the intended Bragg peak position without a magnetic field and its corrected position inside the field (see equation (21)) is non-zero. It ranges from 0.3 mm for 60 MeV and 0.5 T up to 4.3 cm for 250 MeV and 3 T. With the new correction method presented here, the calculated DTA is below 0.1 mm for all studied E_0 and B_0 configurations.

In addition to these differences, we dispute that the beam angle correction can be implemented by a gantry rotation, as stated by Hartman *et al* (2015). To see this, assume for example the intended Bragg peak position (indicated by 'T' in figure 1(a)) to coincide with the gantry's isocenter of rotation. A gantry rotation will then result in a concentric displacement of the actual Bragg peak position U around T, but it will not compensate for the deflection, i.e. render U = T. Transferring this consideration to arbitrary positions of T, it follows that a gantry rotation alone around a fixed isocenter cannot compensate for the proton Bragg peak deflection. Hence we conclude again that the compensation can only be realized by a pencil beam scanning system, which adjusts the entrance angle of the beam.

6. Discussion

6.1. Bragg peak deflection and retraction

The differences we found between the calculated beam deflection Δy and retraction Δx at the Bragg peak can be contributed to the principles of the models as described in sections 2 and 3.

Wolf and Bortfeld (2012) applied a small angle approximation to quantify Δy and Δx in their AI model (see section 2). This approximation becomes inaccurate for large path-lengths. For example, the deflection angle at the phantom entrance position behind the air

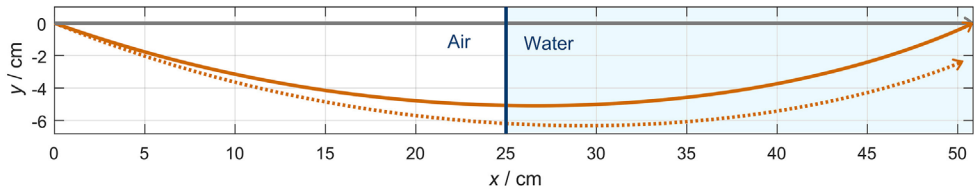

Figure 8. 200 MeV proton beam trajectory through an airgap of thickness $d_{\text{air}} = 25$ cm and a water phantom calculated with RAMDIM. Grey: without magnetic field, orange: $B_0 = 3$ T. The RAMDIM correction method ($\Delta\gamma = 21.6°$, $\Delta E_0 = 3.3$ MeV, solid line) and that of the TG model ($\Delta\gamma = 24.3°$, $\Delta E_0 = 0$, dotted line) have been applied to the beam. The Bragg peak position is indicated by the arrowhead of the trajectory.

gap ($d_{\text{air}} = 25$ cm) is for 200 MeV and 3 T already as high as 41° (see equation (17)). Thus, the assumptions of $\frac{\mathrm{d}y}{\mathrm{d}s} = \sin\phi(s) \approx \phi(s)$ and $\frac{\mathrm{d}x}{\mathrm{d}s} = \cos\phi(s) \approx 1 - \frac{\phi(s)^2}{2}$ constitute a systematic overestimation of the lateral deflection $\Delta y = y(R_0)$ and an underestimation of the longitudinal retraction $\Delta x = R_0 - x(s)$. The deflection angle in water increases with increasing beam energy and magnetic flux density, giving rise to increasing discrepancies relative to the reference data. In addition, the neglection of relativistic effects for the calculation of Δx contributes to an increasing uncertainty with increasing energy. These trends can be clearly observed in figures 4(a) and 5(a). In air, the effect of a decreasing gyroradius with decreasing energy dominates, therefore the travelled pathlength and deflection angle increase with decreasing energy. As the accuracy of the model decreases with increasing deflection angle, this leads to an opposite trend as compared to the lateral deflection, as is appreciated from figures 4(b) and 5(a).

Similarly, we can observe how the approximations brought forward by Hartman *et al* (2015) affect the accuracy of the TG model's predictions. The model neglects retraction, the changing gyroradius due to energy loss and relativistic effects. The accuracy of these approximations decreases with increasing magnetic flux density and proton energy, as is depicted in figure 4. Note that differences in figure 4(b) are solely due to the neglection of relativistic effects, which leads to an underestimation of the gyroradius. The trend to underestimate the deflection in water, as depicted in figure 5(a), can be ascribed to the overestimation of the gyroradius by assuming $r(s) = r_0$. In addition, it was shown that the assumption of a negligible longitudinal Bragg peak retraction exceeds an accuracy of 2 mm already at intermediate energies (see figure 5(a)).

The new model presented in the current work, RAMDIM, does not rely on these assumptions and shows an equally good or better agreement to Monte Carlo results over the whole energy range from 60 MeV to 250 MeV. The remaining differences can be attributed to the approximations of the model, i.e. neglecting scattering, energy-loss fluctuations, range straggling, generation of secondary particles and energy loss in air. Those simplifications were applied to reduce calculation time, but can in principle be included due to the structure of the model being a simplified particle tracking method. The tendency of overestimating lateral deflection and underestimating longitudinal retraction might result from the spectral dispersion of the proton beam due to the magnetic field (Moser 2015), which is not included in the model. Another factor of uncertainty is the proton range R_0, which has been approximated by equation (4) and used as an estimate for the position of the Bragg peak. R_0 deviates from measured Bragg peak positions (Schardt *et al* 2008, Paul 2013) by less than 0.4 mm up to proton energies of 200 MeV.

On the other hand, results obtained by Monte Carlo particle tracking were used in this publication as reference data. However, this approach is theoretical in nature and its accuracy strongly depends on the choice of input parameters and physics models. Consequently, dosimetric measurements have to be carried out for a reliable evaluation of the different models. While this study primarily aimed to introduce the new method, this will be subject to future studies.

For RAMDIM, the particle's equation of motion (equation (1)) has been solved analytically (equation (2)). As an alternative, a full numerical solution by means of a Runge–Kutta method has been proposed recently (Moser 2015). However, as the proton velocity is considered to be constant in each calculation step, the analytical solution applies not only in vacuum but also in media. We therefore consider the Runge–Kutta method to be superfluous in this case, as it will compromise the calculation accuracy and workload.

6.2. Beam correction

The proposed strategy for a compensation of the Bragg peak deflection includes an adjustment of the initial proton beam energy and entrance angle. It was shown that this method effectively repositions the Bragg peak to the intended spot for all studied beam energies and magnetic flux densities. The range difference corresponding to ΔE_0 ranges between 0.01 cm (0.3%) for 60 MeV and 0.5 T and 1.27 cm (3.3%) for 250 MeV and 3 T (see table 2 and equation (4)). The main factor of uncertainty for the proton range in a well-defined geometry is statistical pathlength straggling, and the standard deviation of the range due to this effect ranges between 1.2% for 60 MeV and 1.1% for 250 MeV (Janni 1982, Paganetti *et al* 2012). Being comparably high, the energy correction should therefore not be neglected in MRiPT, especially for higher proton energies and magnetic flux densities.

The reason for the remaining discrepancy of the Bragg peak position corrected by the TG model is seen in the approximations mentioned above. The neglection of retraction constitutes an overestimation of the total path length, and the neglection of relativistic effects leads to an underestimation of the gyroradius and thus an overestimation of the beam deflection. Both approximations result in an overcompensation of the beam deflection.

The calculation time of RAMDIM is strongly decreased as compared to Monte Carlo models. It can be further reduced by using a higher-performant computer and by reducing the required accuracy, which was chosen conservatively in this study.

7. Conclusion and outlook

Although previous work has indicated that there is general consensus that the proton beam trajectory in a water/air phanom setting inside a transverse magnetic field is predictable, our quantitative comparison of the different methods has shown that predictions of different models only agree for certain proton beam energies and magnetic flux densities. Therefore, shortcomings of previously published analytical methods have been analyzed and quantified. The inclusion of critical assumptions and the lack of applicability to realistic, i.e. non-uniform, magnetic flux densities and patient anatomies have been identified as main problems. To overcome these deficiencies, a new model called RAMDIM has been developed and shown to be both less assumptive and more versatile than existing analytical approaches, and faster than Monte Carlo models.

Thus, RAMDIM is useful to get a fast and accurate estimate for the beam deflection and retraction that is to be expected in MRiPT, and for the correction parameters needed for the

compensation thereof. It can help in the planning of experimental setups for dosimetric validation studies of MRiPT, and its simple structure helps to understand underlying physical mechanisms. Furthermore, it can be used as reference solution when setting up a Monte Carlo model or an experimental study. As pointed out by Hartman *et al* (2015), intensity-modulated MRiPT planning can be realized by two Monte Carlo calculation steps—one for selection of beamlets whose deflected Bragg peaks lie inside the target, and one for dose calculation. Thus, another possible application of the model is to replace the first Monte Carlo step in order to reduce the overall calculation time.

We have presented RAMDIM in a simplicistic form for a first approach to the problem of magnetic deflection of the proton beam. However, the structure of the model allows for an easy extension to more realistic cases, especially including range straggling and non-uniform magnetic fields and material compositions. Magnetic flux density vectors of arbitrary distribution and phantom/patient geometries can be included due to the full reconstruction of the trajectory, which provides knowlegde of the proton position at every iteration step. In addition to its reduced amount of approximations, the model thus offers a critically enhanced applicability compared to existing analytical models. Future studies will involve a comprehensive benchmarking of RAMDIM with both Monte Carlo simulations and experimental measurements.

Acknowledgments

The authors would like to thank Wolfgang Enghardt (OncoRay, Dresden, Germany) for useful comments on the manuscript. We furthermore express our gratitude to Marco Schippers (PSI, Villigen, Switzerland) for discussing the initial ideas of the new model.

References

Bortfeld T 1997 An analytical approximation of the Bragg curve for therapeutic proton beams *Med. Phys.* **24** 2024–33

Fallone B G 2014 The rotating biplanar linac-magnetic resonance imaging system *Semin. Radiat. Oncol.* **24** 200–2

Hartman J, Kontaxis C, Bol G H, Frank S J, Lagendijk J J W, van Vulpen M and Raaymakers B W 2015 Dosimetric feasibility of intensity modulated proton therapy in a transverse magnetic field of 1.5 T *Phys. Med. Biol.* **60** 5955–69

ICRU 1993 Stopping powers and ranges for protons and alpha particles *ICRU Report* 49

Jäkel O 2009 Medical physics aspects of particle therapy *Radiat. Prot. Dosim.* **137** 56–166

Janni J F 1982 Proton range-energy tables, 1 keV–10 GeV *At. Data Nucl. Tables* **27** 147–339

Keall P J, Barton M and Crozier S 2014 The Australian magnetic resonance imaging-linac program *Semin. Radiat. Oncol.* **24** 203–6

Lagarias J C, Reeds J A, Wright M H and Wright P E 1998 Convergence properties of the Nelder–Mead simplex method in low dimensions *SIAM J. Optim.* **9** 112–47

Lagendijk J J, Raaymakers B W and van Vulpen M 2014a The magnetic resonance imaging-linac system *Semin. Radiat. Oncol.* **24** 207–9

Lagendijk J J, Raaymakers B W, Van den Berg C A, Moerland M A, Philippens M E and van Vulpen M 2014b MR guidance in radiotherapy *Phys. Med. Biol.* **59** R349–69

Li J S 2015 Investigation of MRI guided proton therapy *Med. Phys.* **42** 3311

Lomax A J 2008 Intensity modulated proton therapy and its sensitivity to treatment uncertainties 2: the potential effects of inter-fraction and inter-field motions *Phys. Med. Biol.* **53** 1043–56

Lühr A, Toftegaard J, Kantemiris I, Hansen D C and Bassler N 2012 Stopping power for particle therapy: the generic library libdEdx and clinically relevant stopping-power ratios for light ions *Int. J. Radiat. Biol.* **88** 209–12

Moser P 2015 Effects on particle beams in the presence of a magnetic field during radiation therapy *Master's Thesis* Technische Universität Wien

Moteabbed M, Schuemann J and Paganetti H 2014 Dosimetric feasibility of real-time MRI-guided proton therapy *Med. Phys.* **41** 111713

Oborn B M, Dowdell S, Metcalfe P E, Crozier S, Mohan R and Keall P J 2015 Proton beam deflection in MRI fields: implications for MRI-guided proton therapy *Med. Phys.* **42** 2113–24

Oborn B M, Dowdell S, Metcalfe P E, Crozier S, Guatelli S, Rosenfeld A B, Mohan R and Keall P J 2016 *MRI Guided Proton Therapy: Pencil Beam Scanning in an MRI Fringe Field (ICTR-PHE Geneva, 15–19 February 2016)*

Paganetti H *et al* 2012 *Proton Therapy Physics* (Boca Raton, FL: CRC Press)

Paul H 2013 *Theory of Heavy Ion Collision Physics in Hadron Therapy* (*Advances in Quantum Chemistry* vol 65) ed D Belkic (New York: Academic)

Raaymakers B, Raaijmakers A J E and Lagendijk J J 2008 Feasibility of MRI guided proton therapy: magnetic field dose effects *Phys. Med. Biol.* **53** 5615–22

Schardt D, Steidl P, Krämer M, Weber U, Parodi K and Brons S 2008 Precision Bragg–Curve measurements for light-ion beams in water *GSI Sci. Rep.* **2007** 373

Schippers J M and Lomax A J 2011 Emerging technologies in proton therapy *Acta Oncol.* **50** 838–50

Wolf R and Bortfeld T 2012 An analytical solution to proton Bragg peak deflection in a magnetic field *Phys. Med. Biol.* **57** N329–37